2012

The nature of Ru-NO bonds in ruthenium tetraazamacrocycle nitrosyl complexes-a computational study

DALTON TRANSACTIONS, CAMBRIDGE, v. 41, n. 24, pp. 7327-7339, MAY, 2012
http://www.producao.usp.br/handle/BDPI/42727

Dalton Transactions

Cite this: *Dalton Trans.*, 2012, **41**, 7327

www.rsc.org/dalton

PAPER

The nature of Ru–NO bonds in ruthenium tetraazamacrocycle nitrosyl complexes—a computational study

Giovanni Finoto Caramori,*[a] André Guilherme Kunitz,[a] Karla Furtado Andriani,[a] Fábio Gorzoni Doro,[b] Gernot Frenking[c] and Elia Tfouni[d]

Received 3rd November 2011, Accepted 29th March 2012
DOI: 10.1039/c2dt12094a

Ruthenium complexes including nitrosyl or nitrite complexes are particularly interesting because they can not only scavenge but also release nitric oxide in a controlled manner, regulating the NO-level *in vivo*. The judicious choice of ligands attached to the [RuNO] core has been shown to be a suitable strategy to modulate NO reactivity in these complexes. In order to understand the influence of different equatorial ligands on the electronic structure of the Ru–NO chemical bonding, and thus on the reactivity of the coordinated NO, we propose an investigation of the nature of the Ru–NO chemical bond by means of energy decomposition analysis (EDA), considering tetraamine and tetraazamacrocycles as equatorial ligands, prior to and after the reduction of the $\{RuNO\}^6$ moiety by one electron. This investigation provides a deep insight into the Ru–NO bonding situation, which is fundamental in designing new ruthenium nitrosyl complexes with potential biological applications.

Introduction

Some decades ago, nitric oxide (NO) was considered a toxic environmental pollutant found primarily in photochemical smog or in exhaust fumes. However, since the discovery that NO is a secretory product in mammalian cells[1–12] it has become one of the most intensively investigated compounds.[13] Nitric oxide has also been classified as one of the most fascinating molecules, playing a relevant role in physiological and pathological process, such as the modulation of the immune and endocrine response, cardiovascular control, regulation of blood pressure, neurotransmission, induction of apoptosis, and inhibition of tumor growth.[7,8] Such biological effects depend, among other factors, on the concentration of NO in the biological milieu. It is recognized that low concentrations of nitric oxide are related to regulatory effects (direct effects) and higher concentrations are related to nitrosative and oxidative stress involving the production of reactive nitrogen and oxygen species (RNOS) (indirect effects).[14]

This scenario has stimulated the development of new storage–release systems, which are able to deliver NO to desired targets controlling its bioavailability.

Among several transition metal complexes that have been developed as metallopharmaceuticals, ruthenium complexes including nitrosyl or nitrite complexes, are particularly interesting because they can not only scavenge but also release nitric oxide in a controlled manner, regulating the NO-level *in vivo*.[15–41] The judicious choice of ligands attached to the [RuNO] core has been shown to be a suitable strategy to modulate NO reactivity in these complexes.[22,26,33,37,38] Ruthenium nitrosyl amines and ruthenium nitrosyl with tetraazamacrocycles are good candidates as NO carriers since they are water soluble, stable in solution and capable of releasing NO by chemical or photochemical activation, not to mention their biological activity.[19,22,35,37–41] The coordinated NO can also exhibit electrophilic behavior, which is modulated by not only by the electron density but also by the NO stretching frequencies. Such complexes display a nitrosonium character of coordinated NO as observed in $[RuNO(NH_3)_5]^{3+}$ and in aqueous solution they may undergo nucleophilic attack for species such as OH^- despite their stability.[37,42,43] The nitrosonium character of coordinated NO in *trans*-$[Ru(NO)L(NH_3)_4]^{q+}$ complexes depends on ligand L *trans* to NO and the presence of macrocycle decreases the electrophilicity of coordinated NO compared to analogous complexes.[37] Although ruthenium nitrosyl amines are robust, the use of saturated macrocyclic polyamines as ligands restricts reactions to the ligands on the axial positions.[38,39] Macrocyclic polyamines present the well-known macrocyclic effect because they can increase the stability of the metal coordination complexes in comparison with the noncyclic tetraamines.[44] Among the macrocyclic polyamines, the 14-membered macrocycle 1,4,8,11-tetraazacyclotetradecane (cyclam or 14-aneN_4) is one of the most commonly employed, being able to coordinate with a huge

[a]*Departamento de Química, Universidade Federal de Santa Catarina, Campus Universitário Trindade, 88040-900 Florianópolis – SC, Brazil. E-mail: caramori@qmc.ufsc.br; Fax: +55-48-3721-6852; Tel: +55-48-3721-6844x239*
[b]*Departamento de Química Geral e Inorgânica, Universidade Federal da Bahia – UFBA, Salvador – BA, Brazil*
[c]*Fachbereich Chemie, Philipps-Universität Marburg, Hans-Meerwein-Strasse, D-35032 Marburg, Germany*
[d]*Departamento de Química, Faculdade de Filosofia Ciências e Letras de Ribeirão Preto, Universidade de São Paulo, Ribeirão Preto, SP, Brazil*

variety of metals, providing not only thermodynamic but also kinetic stability with respect to metal ion dissociation.[45] In general, tetraazamacrocycles, such as cyclam, have applications in different areas, for instance, catalysis, bioinorganic, and medicine.[45–48] The versatility of cyclam also allows *C*- or *N*-functionalization, yielding a huge variety of derivatives, such as monocyclam or bicyclam, which can act as anti-HIV inhibitors, presenting high selectivity.[49–52]

The *trans*-[$Ru^{II}Cl(NO)(cyclam)]X_2$ (X = PF_6^- or ClO_4^-) was isolated and its reactivity studied through spectroscopy, electrochemistry, and photochemistry.[39,40] The results indicated that *trans*-[$Ru^{II}Cl(NO)(cyclam)]^{2+}$ releases NO photochemically without loss of chloride,[25] but after reduction by one electron exhibits a rapid loss of the chloride ion to form the easily oxidized aqua species, *trans*-[$Ru^{II}(OH_2)(NO)(cyclam)]^{2+}$, from which NO is released with a specific rate constant (k_{-NO}) of 6.1×10^{-4} s^{-1}.[39] Although the slow NO release may narrow some biological applications, such as improving the population spike of neurons,[39] it can act as a prodrug for vasodilation with slow blood pressure decrease, as observed in hypertensive male Wistar rats.[19] On replacing cyclam with four amine ligands the resulting ruthenium tetraamine nitrosyl complexes, *trans*-[$Ru^{II}(L)(NO)(NH_3)_4]^{q+}$, present different behavior. After the one electron reduction there are no changes in the coordination sphere, except that of further NO release. For example, when *trans*-[$Ru^{II}(P(OEt)_3(NO)(NH_3)_4)](PF_6)_3$ is reduced at −0.10 V (*vs*. SCE) NO is released with k_{-NO} = 0.97 s^{-1} with formation of the *trans*-[$Ru^{II}(P(OEt_3)(H_2O)(NH_3)_4)]^{2+}$ species.[53] The {RuNO}$^{6/7}$ redox potential of the tetraamine nitrosyl complexes (*trans*-[$Ru^{II}(L)(NO)(NH_3)_4]^{q+}$) (L = Cl^-, isonicotinamide (isn), pyridine (py), H_2O, pyrazine (pz), triethylphosphite ($P(OEt)_3$), 4-picoline (4-pic), 4-chloropyridine (4-Clpy), imidazole (im*C* or im*N*), 4-acetylpyridine (4-acpy) and L-histidine (L-hist)) and k_{-NO} can be tuned by a judicious choice of the *trans* ligand L.[22–37] In previous theoretical studies we have addressed this issue.[54,55]

Unlike *trans*-[$Ru^{II}(L)(NO)(NH_3)_4]^{q+}$, the choice of ligand L *trans* to NO in *trans*-[$Ru^{II}Cl(NO)(cyclam)]^{2+}$ is not easily made feasible due to the remarkable substitution inertness of chloride in the synthetic precursor.[38] As a matter of fact, only chloro complexes, *trans*-[$RuCl(L)(cyclam)]^{q+}$, of cyclam are known.[38] Thus, *N*- (or *C*-) functionalization could be a suitable approach to control the reactivity of coordinated NO. This strategy has been explored using mono-*N*-substituted cyclam with carboxy- or amino-propyl groups.[56–58] It should be stressed that controlling the properties of the complex, such as electronic spectra, reduction potential, and specific rate constant of the release of NO, is crucial for biological applications.[15–23,37,38,59–63]

Tetraazamacrocycles such as cyclam and its derivatives are fairly flexible; they adopt five different configurations, depending on the spatial alignment of the NH protons (Fig. 1). The energies of the different configurations, obtained using molecular mechanics calculations, indicate that the *trans*-III configuration is the most stable in the octahedral coordination and that the *trans*-I configuration becomes more stable relative to the *trans*-III configuration on going from octahedral Ni(II) cyclam complexes to square-planar, square-pyramidal, and trigonal-bipyramidal complexes.[64,65] This was later confirmed by Donnelly and Zimmer[66] who demonstrated the following configurational distribution for Ni(II) substituted cyclam complexes in octahedral

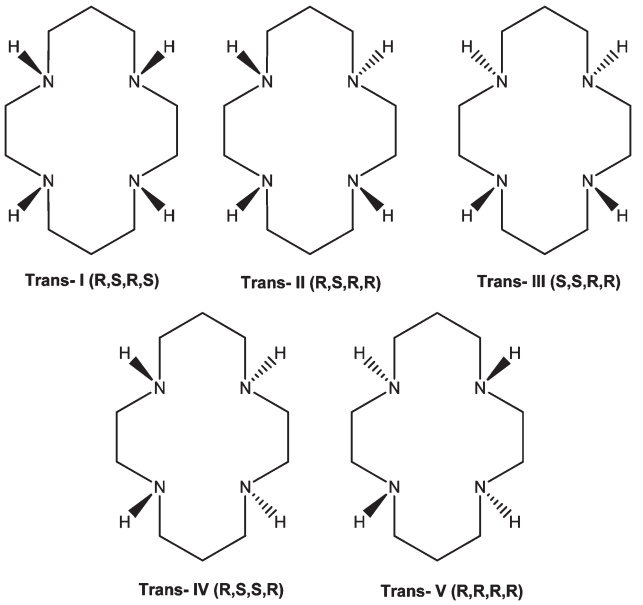

Fig. 1 Configurational isomers of cyclam.

geometry: *trans*-III, 77.8% and *trans*-I, 22.3%. For reasons of stability and symmetry, only the configurational isomers *trans*-III and *trans*-I were considered in this study. Although only ruthenium cyclen (12aneN4 or 1,4,7,10-tetraazacyclododecane) complexes with a *cis* configuration are known,[38,67,68] cyclen derivatives **6–9** were also considered in the same configuration as cyclam and its derivatives **2–5** (Fig. 2) for comparison.

Ruthenium nitrosyl complexes also present photo-induced metastable states, which are linkage isomers in which the nitrosyl is bound through the oxygen atom (MS1) or sideways (η^2) through both oxygen and nitrogen (MS2), as shown in Fig. 2a.[69,70] These kinds of light-induced metastable states were reported for the first time in 1977, in a Mössbauer-spectroscopical study of sodium nitroprusside dihydrate, SNP.[71,72] Subsequently, the presence of the metastable states of SNP was confirmed by differential scanning calorimetry (DSC).[73] These metastable states are populated when samples are irradiated at low temperature with light of the appropriate wavelength, and they are deactivated to the stable ground state (GS) isomer by red de-excitation or by thermal decay.[74,75] The ruthenium nitrosyl complexes for which long-lived metastable states were observed include $K_2[RuCl_5NO]$, $[Ru(NO_2)_4(OH)NO]^{2-}$, $[Ru(CN)_5NO]^{2-}$, $[Ru(py)_4Cl(NO)](PF_6)_2 \cdot 0.5H_2O$ and others.[76–80]

The outstanding structural difference between *trans*-[$Ru^{II}Cl(NO)(cyclam)]^{2+}$ (**2**) and *trans*-[$Ru^{II}Cl(NO)(NH_3)_4]^{2+}$ (**1**) is that the former contains a macrocyclic polyamine (cyclam) while the latter has open-chain amines as equatorial ligands, which, as mentioned above, results in quite different chemical properties.[37,38] In order to understand the influence of different equatorial ligands on the electronic structure of the Ru–NO chemical bonding, and thus on the reactivity of the coordinated NO, we propose an investigation into the nature of the chemical bond Ru–NO, considering tetraamine and tetraazamacrocycles as equatorial ligands, prior to and after the {RuNO}^{6} to {RuNO}^{7} core reduction. This investigation might not only provide a better comprehension of the differences but might also be helpful in

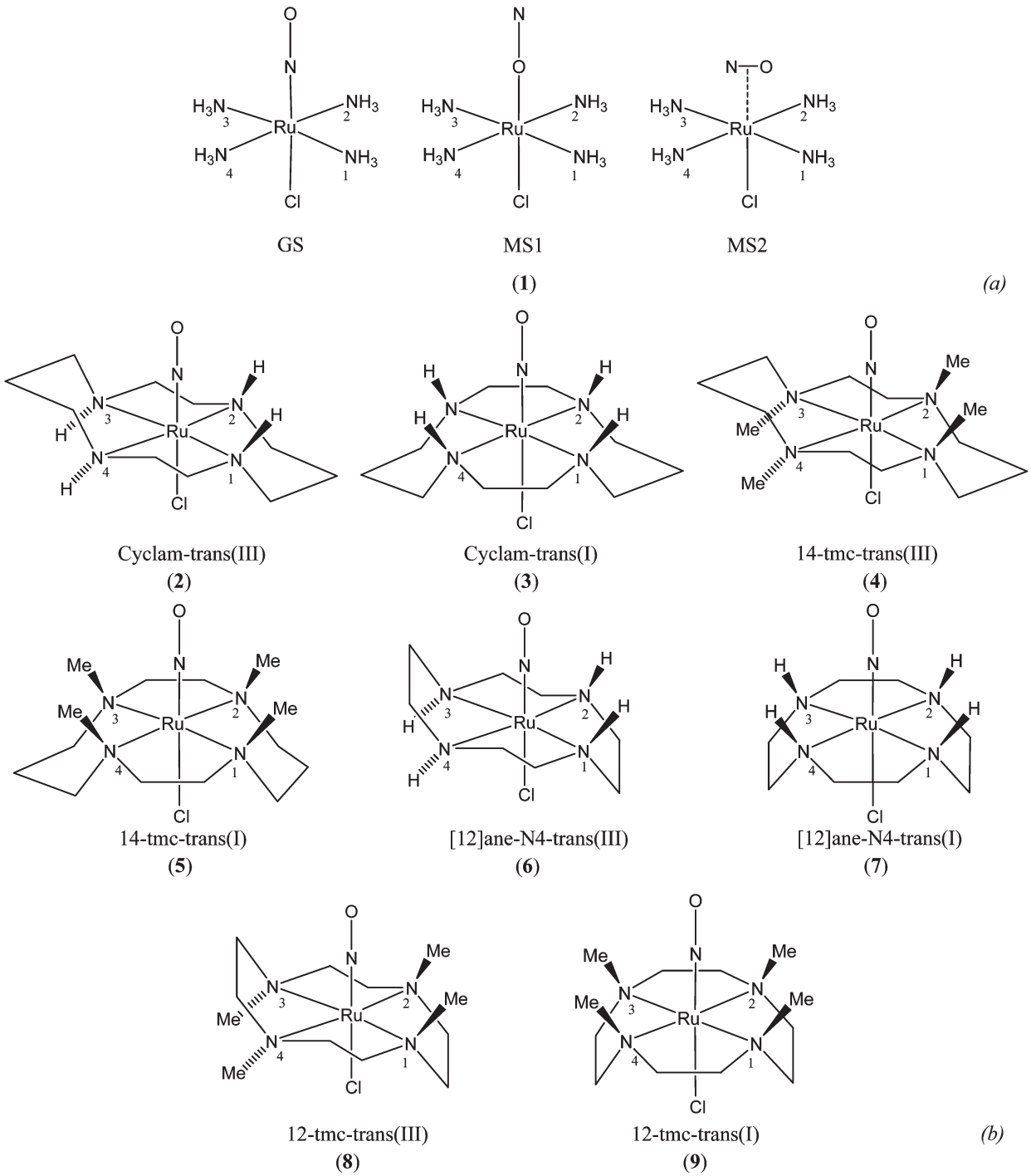

Fig. 2 (a) Ground (GS) and metastable (MS1, MS2) states of *trans*-$[Ru^{II}Cl(NO)(N_4)]^{2+}$; $N_4 = (NH_3)_4$ (**1**). (b) Ground (GS) states of *trans*-$[Ru^{II}Cl(NO)(N_4)]^{2+}$; N_4 = (mac), (mac = cyclam), 1,4,8,11-tetramethyl-1,4,8,11-tetraazacyclotetradecane (1,4,8,11-tetramethylcyclam = 14-tmc), cyclen, or 1,4,7,10-tetramethyl-1,4,7,10-tetraazacyclododecane (1,4,7,10-tetramethylcyclen = 12-tmc) (**2–9**) prior to the reduction of $\{RuNO\}^6$.

designing new ruthenium nitrosyl complexes with potential biological applications. In this context, the tetraazamacrocycles cyclam, 14-tmc, cyclen, and 12-tmc were considered (Fig. 2).

These tetraazamacrocycles allowed us not only to evaluate the influence of the size of the equatorial ligand but also to understand the effects of *N*-substituted derivatives on the electronic structure of the Cl–Ru–NO axis. All chemical bonding analyses were also extended to the metastable states MS1 and MS2.

Methods

The geometries, harmonic frequencies, and bonding characteristics were calculated at the nonlocal DFT level of theory using

the exchange functional of Becke[81] and the correlation functional of Perdew[82] (BP86). Uncontracted Slater-type orbitals (STOs) were used as basis functions for the self consistent field (SCF) calculations.[83] Triple-ζ-quality basis sets were used which were augmented by two sets of polarization functions: p and d functions for the hydrogen atom and d and f functions for the other atoms. This level of theory is denoted as BP86/TZ2P. An auxiliary set of s, p, d, f, and g STOs were used to fit the molecular densities and to represent the Coulomb and exchange potentials accurately in each SCF cycle.[84] Scalar relativistic effects were considered for the transition metals by using the zero-order regular approximation (ZORA).[85–87] The calculations were performed with the ADF-(2005.1) program.[88–90] All structures reported herein were verified as energy minima on the potential energy surface.

The nature of the metal–ligand bond, Ru–NO, was analyzed by means of energy decomposition analysis (EDA), implemented in the ADF program, which was originally developed by Morokuma[91,92] and later modified by Ziegler and Rauk.[93] EDA has been proven to be a reliable and a powerful tool, improving our understanding of the nature of chemical bonding not only in the main group,[94,95] but also in transition-metal compounds.[96,97] Since this method is discussed in detail in the current literature,[84,90] we will describe the theory involved only briefly. The focus of bonding analysis is the instantaneous interaction between the two fragments of the molecule, ΔE_{int}, which is the energy difference between the molecule and its fragments in the frozen geometry of the compound. ΔE_{int} can be decomposed into three different components (eqn (1)),

$$\Delta E_{int} = \Delta E_{elstat} + \Delta E_{Pauli} + \Delta E_{orb} \quad (1)$$

where ΔE_{elstat} is the quasiclassical electrostatic interaction between the fragments and is calculated by considering the frozen electron-density distribution of the fragments in the geometry of the complex. The second term in eqn (1), ΔE_{Pauli}, refers to the repulsive interactions between the fragments due to the fact that two electrons with the same spin cannot occupy the same region in space. It is obtained by enforcing that the Kohn–Sham determinant of the orbitals of the superimposed fragments obeys the Pauli principle by antisymmetrization and renormalization. In the last step of the EDA calculation, the third term of eqn (1), ΔE_{orb}, is obtained by relaxing the molecular orbitals to their optimal forms in order to yield this stabilizing interaction. This term not only incorporates the Heitler–London phenomenon[98] and has the additional contributions of polarization and relaxation, but can also be partitioned into contributions from the orbitals that belong to different irreducible representations of the point group of the interacting system. The interaction energy, ΔE_{int}, together with the term ΔE_{prep}, which is the energy necessary to promote a change in the fragments from their equilibrium geometry and electronic ground state to the geometry and electronic state that they acquire in the compound, can be used to calculate the bond dissociation energy, (eqn (2)). Further details on EDA can be found in the literature.[88–97]

$$-D_e = \Delta E_{prep} + \Delta E_{int}. \quad (2)$$

Results and discussion

Ground and light-induced metastable structures

The chemical bonding analyses of *trans*-$[Ru^{II}Cl(NO)(mac)]^{2+}$ (mac = tetraazamacrocycle = cyclam, 14-tmc, cyclen, or 12-tmc) and *trans*-$[Ru^{II}Cl(NO)(NH_3)_4]^{2+}$ were performed considering structures with the symmetry constraint C_s. This procedure was adopted because EDA enables the partition of the orbital term into contributions that are classified according to the irreducible representations of the local symmetry point group. As the complexes have C_s symmetry, the irreducible representations are a′ and a″. In this case, the orbital interactions can be separated into σ and π contributions. Note that for the GS and MS1 states, the total π-bonding energy is twice the a″ value because the Ru–NO π-bonds in $\{RuNO\}^6$ amines are nearly degenerate. The changes in the energy due to the symmetry constraint are less than 2 kcal mol^{-1}. The structures of octahedral complexes with cyclam and its derivatives were considered in only two configurations; *trans*-III, the most stable, and *trans*-I. In particular, for structures in the ground state (GS), the energy difference between **2** and **3** is 9.0 kcal mol^{-1}, while for **4** and **5** the energy difference lies at around 3.0 kcal mol^{-1}. On the other hand, cyclen and its derivatives show the opposite behavior; that is, the configurational isomer *trans*-I is more stable than *trans*-III.[99] To be more precise, **7** is 2.0 kcal mol^{-1} more stable than **6**, while **9** is 9.0 kcal mol^{-1} more stable than **8**. This is consistent with the fact that, in general, cyclam derivatives are more stable than cyclen, and also that *trans* cyclen was not yet obtained synthetically. This choice makes it possible to investigate the Ru–NO bond in different configurational situations (more or less favorable). The geometric parameters and bond analysis are discussed and compared with *trans*-$[Ru^{II}Cl(NO)(NH_3)_4]^{2+}$ in order to analyze the effects of different equatorial ligands.

Comparing the results of the geometry optimization of the ions prior to the reduction by one electron (*trans*-$[Ru^{II}Cl(NO)(NH_3)_4]^{2+}$ and *trans*-$[Ru^{II}Cl(NO)(cyclam)]^{2+}$) with C_s symmetry, and the available experimental data,[37,39,74,100] it can be observed that the GS bond lengths and angles are fairly well reproduced (Table 1). The shortening of Ru–N bond distance in GS of complex **1** when compared to those of the complexes **2–9** indicates stronger chemical bonds for ruthenium nitrosyls with cyclic amines. Regarding the metastable states (MS1 and MS2) it is possible to observe that the Ru–Cl bond distance increases, indicating that this bond becomes weak. A similar pattern is observed for the Ru–O bond distance but only in the MS2 state.

Although the calculations indicated a weakening of the Ru–Cl bond in tetraazamacrocyclic ligands, the chloride ligand is remarkably inert against substitution in **2** prior to reduction. This ligand inertness has been attributed to the Cl···HN hydrogen bond.[38,39] Complexes in the MS2 state present a slightly different behavior, that is, the Ru–O and Ru–N bond distances are moderately increased and reduced, respectively. The Ru–Cl bond distance variation in MS2 is quite similar to the values observed for GS and MS1 (Table 1 and Fig. 3). Regarding the bonds in the equatorial plane (Ru–N(1), Ru–N(2), Ru–N(3), Ru–N(4)), it is observed that for complexes **2**, **3**, **6**, and **7** in the GS state these bonds are shorter than for **1**. Although there is a decrease in the Ru–N bond lengths for **6**, **7**, **8**, and **9**, it is smaller than

Table 1 Vibrational frequencies ($\nu(NO^+)$, cm^{-1}), bond lengths R (Å), angles (°), and relative energies ΔE_{rel} of GS, MS1, and MS2 (eV) for complexes **1–9**, at BP86/TZ2P

	1			**2**			**3**			**4**			**5**		
	GS	MS1	MS2	GS	MS1	MS2	GS	MS1	MS2	GS	MS1	MS2	GS	MS1	MS2
	C_s	C_s	C_s	C_s	C_s	C_s	C_s	C_s	C_s	C_s	C_s	C_s	C_s	C_s	C_s
ν(NO)	1891	1780	1576	1844	1740	1505	1838	1730	1498	1819	1727	1541	1835	1742	1527
	1888[a]			*1875*[b]											
R(NO)	1.152	1.156	1.193	1.162	1.164	1.207	1.163	1.167	1.209	1.166	1.167	1.200	1.163	1.164	1.202
	1.08[c]			*1.128(4)*[d]											
R(RuN)	1.780	—	1.941	1.762	—	1.926	1.762	—	1.925	1.759	—	1.936	1.756	—	1.927
	1.79 (1)			*1.747(4)*											
R(RuO)	—	1.886	2.207	—	1.860	2.230	—	1.859	2.232	—	1.856	2.225	—	1.853	2.234
R(RuCl)	2.296	2.260	2.276	2.334	2.287	2.296	2.330	2.287	2.293	2.314	2.277	2.279	2.343	2.301	2.313
	2.355(3)			*2.327(1)*											
R(RuN(1))	2.157	2.156	2.181	2.147	2.138	2.124	2.149	2.136	2.174	2.193	2.188	2.186	2.198	2.189	2.189
	2.101(8)			*2.097(4)*											
R(RuN(2))	2.159	2.158	2.159	2.147	2.138	2.124	2.149	2.136	2.174	2.193	2.188	2.186	2.198	2.189	2.189
	2.109(7)			*2.093(4)*											
R(RuN(3))	2.163	2.160	2.162	2.122	2.120	2.148	2.148	2.141	2.121	2.199	2.196	2.256	2.207	2.201	2.262
	2.101(8)			*2.088(4)*											
R(RuN(4))	2.159	2.158	2.159	2.122	2.120	2.148	2.147	2.141	2.121	2.199	2.196	2.256	2.207	2.201	2.262
	2.109(7)			*2.089(4)*											
∠RuNO	179.9	—	86.0	179.5	—	87.6	177.7	—	87.7	178.0	—	88.7	178.4	—	88.0
	174.9(3)			*178.0*											
∠RuON	—	179.8	61.3	—	178.5	59.6	—	178.3	59.5	—	178.7	59.1	—	178.6	60.0
ΔE_{rel}	0.00	1.80	1.60	0.0	1.88	1.67	0.0	1.86	1.69	0.00	1.85	2.05	0.00	1.86	1.91

	6			**7**			**8**			**9**		
	GS	MS1	MS2	GS	MS1	MS2	GS	MS1	MS2	GS	MS1	MS2
	C_s	C_s	C_s	C_s	C_s	C_s	C_s	C_s	C_s	C_s	C_s	C_s
ν(NO)	1850	1744	1519	1856	1751	1505	1822	1726	1561	1847	1751	1527
R(NO)	1.161	1.163	1.204	1.160	1.162	1.206	1.165	1.166	1.196	1.161	1.162	1.201
R(RuN)	1.765	—	1.940	1.763	—	1.927	1.765	—	1.962	1.756	—	1.926
R(RuO)	—	1.866	2.222	—	1.861	2.226	—	1.865	2.262	—	1.853	2.235
R(RuCl)	2.382	2.315	2.340	2.388	2.337	2.347	2.344	2.300	2.308	2.403	2.352	2.371
R(RuN(1))	2.064	2.059	2.046	2.075	2.068	2.058	2.101	2.100	2.093	2.107	2.100	2.104
R(RuN(2))	2.064	2.059	2.046	2.075	2.068	2.058	2.101	2.100	2.093	2.107	2.100	2.104
R(RuN(3))	2.047	2.046	2.066	2.072	2.066	2.087	2.116	2.111	2.156	2.106	2.100	2.140
R(RuN(4))	2.049	2.046	2.066	2.072	2.066	2.087	2.116	2.111	2.156	2.106	2.100	2.140
∠RuNO	176.7	—	86.6	179.0	—	87.4	175.4	—	88.0	179.3	—	88.1
∠RuON	—	176.3	60.6	—	179.3	59.8	—	176.4	60.1	—	179.4	59.5
ΔE_{rel}	0.00	1.87	1.81	0.00	1.92	1.75	0.00	1.81	2.14	0.00	1.89	1.92

[a] Experimental ν_{NO} value from ref. 45, taken in KBr pellet. [b] Experimental ν_{NO} value from ref. 39, taken in KBr pellet. [c] Experimental data from ref. 74 and 100. [d] Experimental data from ref. 39.

expected for a 12-membered ring, and should result in thermodynamically less stable complexes. Nevertheless, the *N*-substituted complexes, **4**, **5**, **8**, and **9**, present slightly longer equatorial bond lengths compared with **1**. This is a direct consequence of the inductive effect of the methyl groups. Complexes in the MS1 and MS2 metastable states exhibit a similar trend, whereas this is not so pronounced for **8** and **9**.

As in the case of **1**, the complexes **2–9** in the GS and MS1 states also present a pseudo-octahedral arrangement around the metal atom and the angles Ru–N–O and Ru–O–N are close to or equal to 180°, indicating the nitrosonium character in the NO ligand. However, complexes **2–9** show a reduction in the Ru–N–O and Ru–O–N angles in comparison with the respective angles of **1**. The most marked changes are observed for complexes **6** and **8**, for which the variations are around 3.5 and 4.5 degrees. According to these angles, the [Ru^{II}–NO^+] canonical form predominates in the {RuNO}^{6} moiety (other canonical forms are [Ru^{III}–NO^0] and [Ru^{IV}–NO^-]).[37,38,101–104] The predominance of the [Ru^{II}–NO^+] canonical form has been further supported by extensive reactivity data for $[Ru(NO)(NH_3)_5]^{3+}$ provided by Bottomley[42] and Lehnert *et al.* through detailed spectroscopic and electronic structural evidences.[43]

It is also interesting to note that, according to theoretical calculations and experimental data, the [$Fe^{II}NO^+$] predominates in ferric heme-nitrosyls.[104]

Prior to reduction by one electron, the N–O bond distances are only slightly influenced by the nature of the equatorial ligands. In comparison with **1**, the N–O bond lengths for complexes **2–9** become slightly longer (Table 1 and Fig. 4). These results are also confirmed by the relative N–O stretching frequencies (ν_{NO}) of complexes **2–9**, which become smaller than for **1** (Fig. 5). The calculated ν_{NO} for the non reduced species are very close to the available experimental values[38,105] (Table 1). Going from **1** to **2**, the drop in the calculated N–O stretch is 47 cm^{-1}, when experimentally it is just 13 cm^{-1}. In principle, it can be attributed to the density functional employed. Additional calculations

employing functionals such as OLYP and B3LYP revealed a similar trend, 39 cm^{-1} and 40 cm^{-1}, respectively. However, by comparing the calculated N–O bond distance in **1** and **2**, we note similar values, 1.152 Å and 1.162 Å, while the values observed experimentally are 1.08 Å and 1.128Å, respectively. Therefore, the observed discrepancies can not only be attributed to the failures of DFT to evaluate Hessian matrix, but also to the intrinsic differences between structures considered in calculations and those considered to perform spectroscopic analysis.

As performed for the ions *trans*-$[Ru^{II}Cl(NO)(NH_3)_4]^{2+}$ and *trans*-$[Ru^{II}Cl(NO)(mac)]^{2+}$, **1–9**, with C_s symmetry, a similar analysis was carried out considering the reduced ions *trans*-$[Ru^{II}Cl(NO)(NH_3)_4]^{+}$ and *trans*-$[Ru^{II}Cl(NO)(mac)]^{+}$, **1a–9a** (Scheme 1), and performing unrestricted spin calculations.[106] The reduction was modelled by the addition of one electron to the π* N–O orbital, as predicted by the reduction product analysis in voltammetric experiments and calculations for some Ru nitrosyls.[100,107,108] EPR experiments[39,109] indicate that there is a considerable energy difference between the two π* orbitals of NO, which is confirmed by the strong anisotropy in the *g* matrix, indicating a bent structure for the Ru–NO bond (Ru–N–O or Ru–O–N angles are approximately 140°), as demonstrated through our calculations for the GS and MS1 states of *trans*-$[Ru^{II}Cl(NO)(NH_3)_4]^{+}$ and *trans*-$[Ru^{II}Cl(NO)(mac)]^{+}$, **1a–9a** (Table 2, Scheme 1).

Due to the reduction, all N–O bonds are lengthened, which can be interpreted as a direct consequence of the decrease in the bond orders. This finding is also confirmed by the decrease in the NO vibrational stretching frequencies, ν_{N-O}, in comparison with the ν_{N-O} values for the *trans*-$[Ru^{II}Cl(NO)(NH_3)_4]^{2+}$ and *trans*-$[Ru^{II}Cl(NO)(mac)]^{2+}$, **1–9**, complexes. The shifts of the calculated stretching frequency, ν_{N-O}, values of the reduced

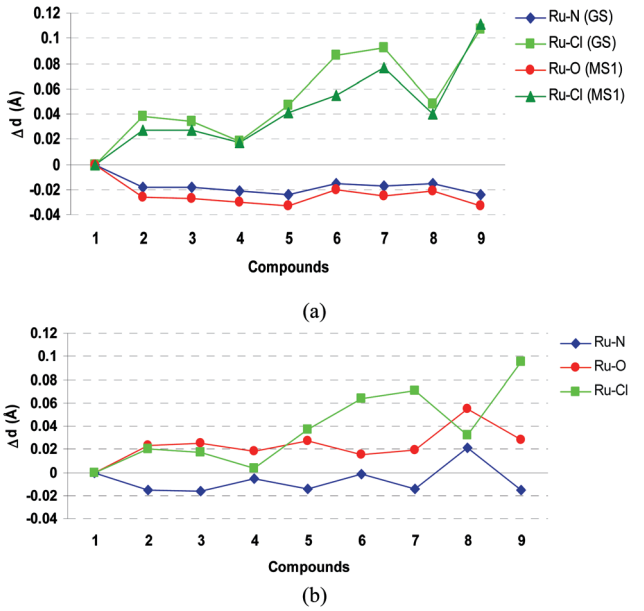

Fig. 3 Relative bond lengths for complexes **2–9** in (a) GS and MS1 states (b) MS2 state.

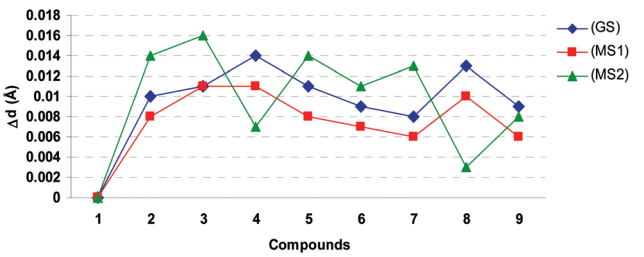

Fig. 4 Variations in the N–O bond lengths of **2–9** in relation to complex **1** prior to reduction by one electron.

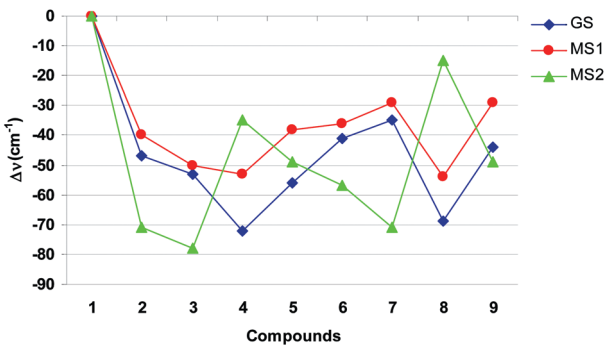

Fig. 5 Variations in the N–O stretching frequencies of **2–9** in relation to complex **1** prior to reduction by one electron.

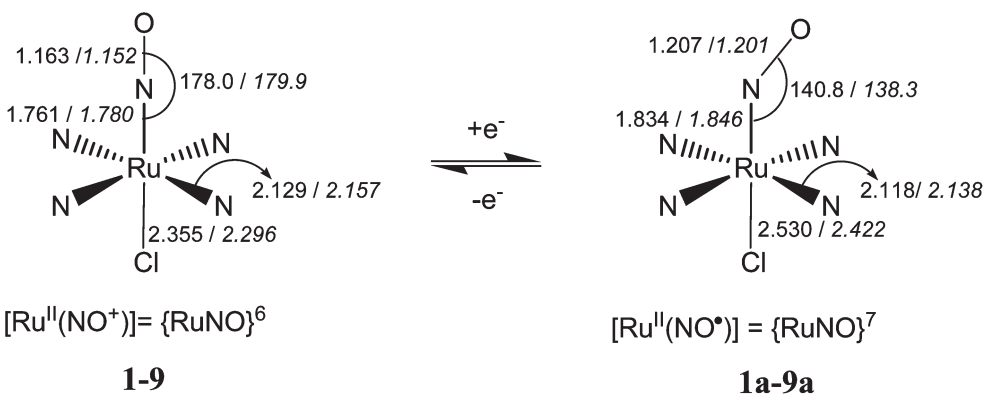

Scheme 1 Schematic representation of the reduction of $\{RuNO\}^6$ core species (**1–9**), generating the reduced $\{RuNO\}^7$ species (**1a–9a**), in which the average metric parameters for the macrocyclic N_4 ligands and N_4 amine (*in italics*) in GS state are represented.

Table 2 Vibrational frequencies ($\nu(NO^0)$, cm^{-1}), bond lengths R (Å), angles (°), and relative energies ΔE_{rel} of GS, MS1, and MS2 (eV) for complexes **1a–9a**, at BP86/TZ2P

	1a			**2a**			**3a**			**4a**			**5a**		
	GS	MS1	MS2	GS	MS1	MS2	GS	MS1	MS2	GS	MS1	MS2	GS	MS1	MS2
ν(NO)	C_s 1591	C_s 1518	C_s 1350	C_s 1546 *1853*[a] *1830*[b]	C_s 1474	C_s 1336	C_s 1553	C_s 1465	C_s 1341	C_s 1576	C_s 1496	C_s 1390	C_s 1589	C_s 1514	C_s 1365
R(NO)	1.201	1.202	1.262	1.211	1.213	1.264	1.210	1.214	1.263	1.207	1.209	1.249	1.204	1.205	1.255
R(RuN)	1.846	—	2.059	1.835	—	2.072	1.833	—	2.065	1.836	—	2.09	1.829	—	2.068
R(RuO)	—	1.981	2.096	—	1.963	2.106	—	1.960	2.108	—	1.970	2.100	—	1.962	2.090
R(RuCl)	2.422	2.352	2.337	2.463	2.375	2.367	2.480	2.395	2.375	2.475	2.390	2.371	2.547	2.435	2.420
R(RuN(1))	2.138	2.137	2.155	2.126	2.111	2.119	2.126	2.110	2.120	2.186	2.177	2.196	2.194	2.178	2.196
R(RuN(2))	2.153	2.145	2.136	2.126	2.111	2.119	2.126	2.110	2.120	2.186	2.177	2.196	2.194	2.178	2.196
R(RuN(3))	2.156	2.145	2.149	2.115	2.111	2.125	2.140	2.130	2.141	2.201	2.189	2.231	2.206	2.193	2.244
R(RuN(4))	2.153	2.145	2.136	2.115	2.111	2.125	2.120	2.130	2.141	2.201	2.189	2.231	2.206	2.193	2.244
∠RuNO	138.3	—	73.9	137.3	—	73.9	137.9	—	74.2	145.5	—	73.4	143.6	—	73.4
∠RuON	—	138.9	70.9	—	136.0	70.9	—	137.7	70.5	—	149.5	72.0	—	146.3	71.5
ΔE_{rel}	0.00	1.45	0.93	0.00	1.44	0.95	0.00	1.47	0.86	0.00	1.45	1.36	0.00	1.07	0.85

	6a			**7a**			**8a**			**9a**		
	GS	MS1	MS2	GS	MS1	MS2	GS	MS1	MS2	GS	MS1	MS2
ν(NO)	C_s 1553	C_s 1460	C_s 1352	C_s 1582	C_s 1488	C_s 1334	C_s 1578	C_s 1490	C_s 1411	C_s 1599	C_s 1511	C_s 1359
R(NO)	1.210	1.214	1.259	1.205	1.209	1.263	1.206	1.209	1.244	1.202	1.205	1.256
R(RuN)	1.840	—	2.094	1.830	—	2.059	1.846	—	2.133	1.823	—	2.065
R(RuO)	—	1.974	2.105	—	1.961	2.101	—	1.983	2.122	—	1.962	2.094
R(RuCl)	2.500	2.384	2.408	2.580	2.451	2.430	2.507	2.407	2.399	2.691	2.492	2.483
R(RuN(1))	2.049	2.039	2.047	2.060	2.048	2.056	2.098	2.096	2.102	2.104	2.092	2.109
R(RuN(2))	2.049	2.039	2.047	2.060	2.048	2.056	2.098	2.096	2.102	2.104	2.092	2.109
R(RuN(3))	2.046	2.042	2.054	2.072	2.061	2.063	2.117	2.106	2.140	2.110	2.095	2.128
R(RuN(4))	2.046	2.042	2.054	2.072	2.061	2.063	2.117	2.106	2.140	2.110	2.095	2.128
∠RuNO	136.5	—	73.0	138.4	—	74.1	144.0	—	72.5	143.1	—	73.7
∠RuON	—	134.0	72.1	—	137.0	70.5	—	148.0	73.5	—	145.3	71.1
ΔE_{rel}	0.00	1.40	1.08	0.0	1.51	0.94	0.00	1.39	1.47	0.00	1.50	1.27

[a] Ref. 39 in KBr. [b] Ref. 38 in acetonitrile.

species with regard to the parent complexes are comparable to those reported and/or calculated elsewhere for other complexes with different metals and/or ligands.[110–112] However, the infrared spectrum of *trans*-$[Ru^{II}Cl(NO)(mac)]^{2+}$ after reduction shows a peak at 1853 cm^{-1} in KBr and 1830 cm^{-1} in acetonitrile,[38] assigned to either the coordinated nitrosonium in *trans*-$[Ru^{II}(OH)(NO)(mac)]^{2+}$ as a possible result of subsequent reactions after reduction of *trans*-$[Ru^{II}Cl(NO^0)(mac)]^{+}$ or to the coordinated NO^0 in *trans*-$[Ru^{II}Cl(NO^0)(mac)]^{+}$.[38,39] The calculated $\nu_{N–O}$ value of the reduced *trans*-$[Ru^{II}Cl(NO)(mac)]^{+}$ (1546 cm^{-1}, Table 2) is much lower than observed, indicating that the assignment would be more consistent with *trans*-$[Ru^{II}(OH)(NO)(mac)]^{2+}$. After the reduction, it is observed that not only the Ru–NO but also the Ru–Cl bond lengths for GS and MS1 increase. This increase, considering a $[Ru^{III}–NO^0]$ canonical form, is consistent with a smaller charge attraction in the reduced species, $\{RuNO\}^7$, and is a direct consequence of the Jahn–Teller effect along with the *trans* effect of NO^0 ligand in $\{RuNO\}^7$ species.[39,113,114] Much more detail for this effect has been provided for ferrous heme-nitrosyl, $\{FeNO\}^7$, by means of structural as well as spectroscopical characterization. For instance, an $Fe–N_{IM}$ stretching mode of only 149 cm^{-1} in [Fe(TPP)(MI)(NO) (TPP = tetraphenylporphyrin dianion, MI = 1-methylimidazole) underlines the *trans* interaction of MI with bound NO^0.[115]

This lengthening is also consistent with the fast chloride release (k_{-Cl} = 1.5 s^{-1}) observed for **2** after the one-electron reduction in solution. Comparing the reduced species $\{RuNO\}^7$, **1a–9a**, an increase in the Ru–Cl distance is observed for the complexes containing macrocyclic ligands, **2a–9a**, in comparison with **1a**. This increase is not dependent on the metastable state. On the other hand, the Ru–N and Ru–O bond lengths of the Ru–NO moiety for the GS or MS1 metastable states either remain constant or change slightly, depending on the nature of the tetraazamacrocycle (Table 2 and Fig. 6). The **2a–9a** N–O bond distances presented only small changes in comparison with **1a**. Regarding the bonds in the equatorial plane (Ru–N(1), Ru–N(2), Ru–N(3), Ru–N(4)), it is observed that for complexes **2a**, **3a**, **6a**, and **7a** in the GS state they are shorter than for **1a**. For the *N*-substituted complexes, **4a**, **5a**, **8a**, and **9a**, the equatorial bond lengths are slightly longer than the bond lengths of **1**. This is a direct consequence of the inductive effect of the methyl groups. Complexes in the MS1 and MS2 metastable states exhibit a similar trend, whereas this is not so pronounced for **8a** and **9a**. Therefore, the geometrical parameters indicated that complexes with tetraazamacrocycles as equatorial ligands exhibit

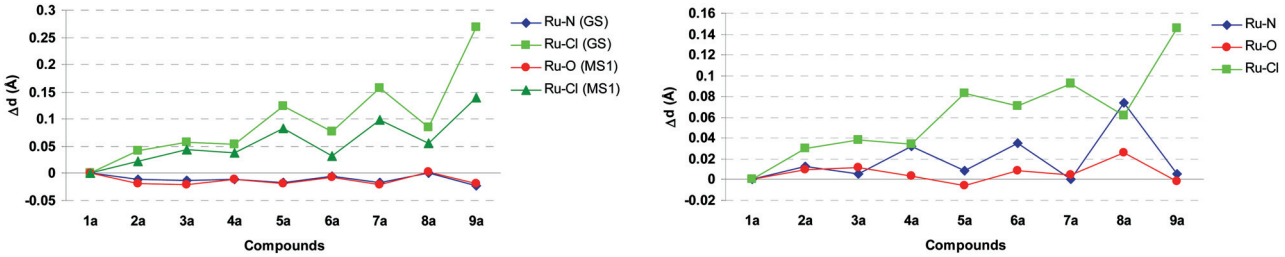

(a) (b)

Fig. 6 Relative bond lengths of complexes **2a–9a** in (a) GS and MS1 states (b) MS2 state.

an increase in the Ru–Cl bond length and contraction of the Ru–NO, Ru–ON, and Ru–N(*i*), which represents the Ru–N(1), Ru–N(2), Ru–N(3), and Ru–N(4) bonds respectively. This behavior is observed not only prior to but also after the reduction by one electron of the NO group. The results indicate that in the presence of equatorial ligands the Ru–Cl bonds become weak while the Ru–NO, Ru–ON, and Ru–N(*i*) bonds become stronger. In addition, the methyl substituents of *N*-substituted tetraazamacrocycles increase the equatorial bond distances, Ru–N(*i*), as a direct consequence of the inductive effect of the methyl groups.

Bonding analysis

EDA of *trans*-[Ru^{II}Cl(NO)(NH$_3$)$_4$]$^{2+}$ and *trans*-[Ru^{II}Cl(NO)(mac)]$^{2+}$. Table 3 shows the EDA results and the calculated Hirshfeld charges[116] of the NO$^+$ group (f2) (assuming a [Ru^{II}–NO$^+$] canonical form) and the remaining metal fragment in the d^6 low-spin state for the complexes [Ru^{II}Cl(NH$_3$)$_4$]$^+$ and [Ru^{II}Cl(mac)]$^+$, which is referred to as fragment (f1). The ΔE_{int} values indicate that the NO$^+$ group binds more strongly (more negative ΔE_{int}) with the remaining metal fragments containing tetraazamacrocycles, **2–9**, than with metal fragments with tetraamines, **1**. This trend occurs not only for complexes in the ground state (GS), but also for the complexes in metastable states (MS1 and MS2). Notwithstanding the fact that fragments (f1) and (f2) have similar charges for all complexes **1–9**, the complexes with tetraazamacrocycles **2–9** exhibit more negative ΔE_{int} values than **1**. This is attributed mainly to the orbital term, ΔE_{orb}, which is more negative for **2–9** than for **1**. The strength of the interaction between NO$^+$ and metal fragments with tetraazamacrocycles is also confirmed by the more negative values of the bond dissociation energy, $-D_e$, in comparison with **1**. In addition, a reduction in the positive electrostatic term, ΔE_{elstat}, is noted for complexes **2–9**. This indicates that the Coulomb repulsion between the NO$^+$ and the metal fragments with tetraazamacrocycles is minimized in comparison with the same repulsion between NO$^+$ and the metal fragment with tetraamine, **1**.

EDA separates the orbital term into contributions that are classified according to the irreducible representations of the local point group symmetry. As the complexes have C_s symmetry, the irreducible representations are a′ and a″. In this case, the orbital interactions can be separated into σ and π. Note that for the GS and MS1 states, the total π-bonding energy is twice the a″ value because the π-bonds in {RuNO}^{6} are nearly degenerate, as shown in our previous work.[54] The contribution of the second in-plane π-bond in {RuNO}^{6} is included in the a′ orbital term. However, in the case of MS2, this separation is not possible due to the bent arrangement of the NO ligand and therefore there is a strong mixture of σ and in-plane π interactions belonging to the irreducible representation a′.[54] The π back-donation, ΔE_π, is the most important contribution to the orbital interaction, ΔE_{orb}, representing more than 80%, while the σ contribution, ΔE_σ, represents less than 20% of the total orbital contribution. The large domination of the Ru–NO bond in {RuNO}^{6} species by Ru–NO π backbonding was also observed for [Ru(NO)(NH$_3$)$_5$]$^{3+}$.[45]

It is important to note that the complexes **2–9** present an increase in the ΔE_π and a decrease of the ΔE_σ contributions. This increase in ΔE_π suggests higher electron density over the NO ligand which is consistent with the ν(NO) stretching <1900 cm^{-1} and lower electrophilicity of **2**, for which experimental data are available.[38,39] In particular, the *N*-substituted tetraazamacrocycles, **4**, **5**, **8**, and **9**, exhibit the most negative values of ΔE_π, which is a direct consequence of the inductive effect of the methyl substituents, which increases the electronic density in the equatorial plane through electron density donation (inductive effect).

Consequently, the π back-donation becomes slightly more effective for these complexes than for the non-substituted tetraazamacrocycles. As shown for *trans*-[Ru(L)(NO)(NH$_3$)$_4$]$^{q+}$,[38,39,54] the degree of Ru$_{d\pi-\pi^*}$NO back-donation and thus the electron content at NO can be correlated to its reduction potential and electrophilicity. Since *N*-alkyl substitution suggests an increase in the d$_{\pi-\pi^*}$NO back donation in the tetraazamacrocyclic ruthenium nitrosyl complexes investigated in this study, it seems reasonable to assume that the adequate choice of the degree of *N*-substitution (mono, bi, tri or tetra-substitution) and type (electron donating or acceptor) of *N*-substituents would be a suitable strategy for controlling the reactivity of coordinated nitrosyl and, as a consequence, for designing new nitrosyl complexes based on tetraazamacrocyclic ligands as NO-carriers for potential biological applications. Regarding the MS2 state, despite the fact that it is not possible to split the large values of $\Delta E_{(A')}$ into σ and π contributions, it is possible to assert that in bending the NO group, the overlap between the metal orbitals and the NO π* orbitals is minimized in comparison with the overlaps of the GS and MS1 states.[54] The large values of ΔE_{prep}, for MS2 (22.6–35.0 kcal mol^{-1}), in comparison with the values obtained for GS and MS1 (10.5–19.6 kcal mol^{-1}), are related to the deformation of the fragment geometries from the equilibrium structures to the complexes, mainly in relation to the NO$^+$ group.

Table 3 EDA of axial NO^+ of *trans*-$[Ru^{II}(Cl)NO(NH_3)_4]^{2+}$, (**1**) and *trans*-$[Ru^{II}(Cl)NO(mac)]^{2+}$ complexes **2–9** at BP86/TZ2P[a]

	1			**2**			**3**			**4**			**5**		
	GS	MS1	MS2	GS	MS1	MS2	GS	MS1	MS2	GS	MS1	MS2	GS	MS1	MS2
	C_s	C_s	C_s	C_s	C_s	C_s	C_s	C_s	C_s	C_s	C_s	C_s	C_s	C_s	C_s
ΔE_{int}	−69.2	−28.2	−46.7	−94.9	−50.9	−68.9	−97.8	−54.3	−72.0	−97.3	−54.0	−65.8	−97.7	−54.1	−68.0
ΔE_{pauli}	144.2	83.1	141.2	157.5	96.0	156.1	157.1	95.3	148.3	170.4	107.7	161.2	166.1	103.2	152.1
ΔE_{elstat}	46.3	74.5	59.6	38.5	68.9	49.9	37.4	68.0	54.1	34.2	64.5	47.3	33.3	63.6	50.0
ΔE_{orb}	−259.6	−185.8	−247.5	−290.9	−215.8	−274.9	−292.3	−217.6	−274.3	−301.9	−226.2	−274.4	−297.1	−220.9	−270.1
$\Delta E_{(A')}$	−151.3	−106.3	−180.9	−166.4	−122.0	−194.4	−166.8	−123.0	−193.3	−171.5	−127.1	−191.0	−169.5	−124.5	−191.8
$\Delta E_{(A'')}$	−108.3	−79.6	−66.5	−124.5	−93.8	−80.5	−125.5	−94.7	−81.0	−130.4	−99.1	−83.4	−127.6	−96.4	−78.3
ΔE_{σ}	−43.0	−26.6	—	−41.9	−28.2	—	−41.3	−28.2	—	−41.1	−28.0	—	−41.9	−28.1	—
	17%	14%		14%	13%		14%	13%		14%	12%		14%	13%	
ΔE_{π}[b]	−216.6	−159.2	—	−249.0	−187.6	—	−251.0	−189.4	—	−260.8	−198.2	—	−255.2	−192.8	—
	83%	86%		86%	87%		86%	87%		86%	88%		86%	87%	
$-D_e$	−58.7	−17.3	−24.1	−79.7	−38.7	−41.3	−82.1	−39.2	−43.3	−78.8	−36.1	−31.6	−80.5	−37.7	−36.6
ΔE_{prep}	10.5	10.9	22.6	15.2	12.2	27.6	15.7	15.2	28.7	18.5	17.9	34.2	17.2	16.4	31.4
$q(f1)$[c]	1.81	1.77	1.82	1.88	1.85	1.87	1.89	1.87	1.90	1.88	1.85	1.86	1.88	1.85	1.86
$q(f2)$	0.19	0.23	0.18	0.12	0.15	0.13	0.11	0.13	0.10	0.12	0.15	0.14	0.12	0.15	0.14

	6			**7**			**8**			**9**		
	GS	MS1	MS2	GS	MS1	MS2	GS	MS1	MS2	GS	MS1	MS2
	C_s	C_s	C_s	C_s	C_s	C_s	C_s	C_s	C_s	C_s	C_s	C_s
ΔE_{int}	−89.8	−44.1	−60.4	−95.2	−49.7	−67.2	−91.1	−48.1	−57.2	−97.2	−52.5	−66.4
ΔE_{pauli}	154.5	95.2	147.3	150.5	89.8	141.6	168.0	105.1	149.6	159.8	98.1	146.7
ΔE_{elstat}	42.1	71.7	57.3	39.2	68.8	56.1	37.6	67.7	55.0	36.2	65.9	53.0
ΔE_{orb}	−286.4	−211.0	−265.0	−284.9	−208.3	−264.9	−296.7	−220.9	−261.8	−293.2	−216.6	−266.1
$\Delta E_{(A')}$	−163.1	−117.6	−185.8	−161.9	−116.0	−188.0	−168.1	−123.0	−180.3	−166.4	−120.4	−189.1
$\Delta E_{(A'')}$	−123.3	−93.4	−79.2	−123.0	−92.4	−76.9	−128.6	−97.9	−81.5	−126.8	−96.1	−77.0
ΔE_{σ}	−39.8	−24.2	—	−38.9	−23.5	—	−39.5	−25.1	—	−39.6	−24.4	—
	14%	12%		14%	11%		13%	11%		14%	11%	
ΔE_{π}[b]	−246.6	−186.8	—	−246.0	−184.8	—	−257.2	−195.8	—	−253.6	−192.2	—
	86%	88%		86%	89%		87%	89%		86%	89%	
$-D_e$	−71.7	−28.5	−29.9	−80.0	−35.7	−39.7	−71.4	−29.8	−22.2	−80.2	−36.8	−35.9
ΔE_{prep}	18.1	15.6	30.5	15.2	14.0	27.5	19.6	18.3	35.0	17.0	15.7	30.5
$q(f1)$[c]	1.87	1.84	1.87	1.87	1.84	1.88	1.88	1.85	1.86	1.87	1.84	1.86
$q(f2)$	0.13	0.16	0.13	0.13	0.16	0.12	0.12	0.15	0.14	0.13	0.16	0.14

[a] Energy contributions in kcal mol^{-1}. [b] Percentage contribution to the total orbital interactions, ΔE_{orb}. [c] Hirshfeld charges for fragments.

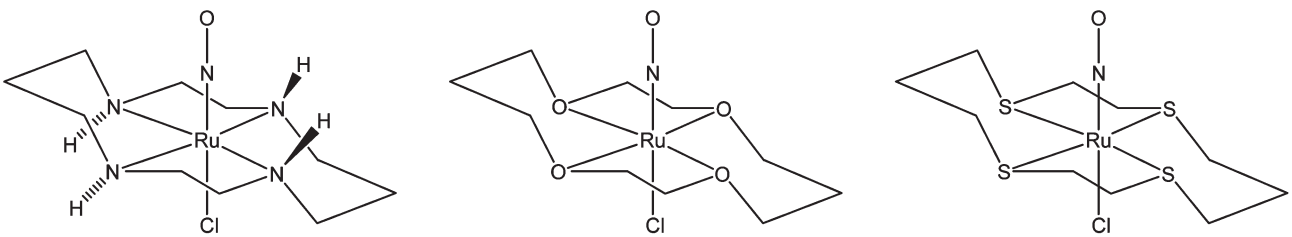

Fig. 7 Ground state structures of *trans*-$[Ru^{II}Cl(NO)(A_4)]^{2+}$; ($A_4$ = tetracoordinated equatorial ligands), A_4 = (1,4,8,11-tetraazacyclotetradecane) (**2**), A_4 = (1,4,8,11-tetraoxacyclotetradecane) (**2b**), and A_4 = (1,4,8,11-tetrathiacyclotetradecane) (**2c**).

Complexes **2–9** have larger ΔE_{prep} values than complex **1**. This is attributed to the fact that deformation of the tetraazamacrocycles in metal fragments of **2–9** is much more intense than that of the tetraamine in fragments of **1**. Despite the increase in the Pauli repulsion term, ΔE_{Pauli}, for complexes **2–9**, the differences observed for ΔE_{int} are mainly due to the electrostatic and orbital contributions. The Pauli repulsion term, ΔE_{Pauli}, independently of the nature of the equatorial ligand, has the trend GS > MS2 > MS1. The EDA results also show that the size of the tetraazamacrocycles affect, to some extent, the EDA values. Comparing the EDA results of complexes **2** and **3** (cyclam) with **6** and **7** (cyclen), it is observed that complexes **2** and **3** have more negative ΔE_{int} and ΔE_{orb} and more positive ΔE_{Pauli} values than complexes **6** and **7**, suggesting the metal centre of the former complexes is richer in electrons than the latter.

In order to provide additional insight about the effects of tetracoordinated equatorial ligands, A_4, on the Ru–NO bonding situation, two different ligands were considered (1,4,8,11-tetraoxacyclotetradecane and 1,4,8,11-tetrathiacyclotetradecane) (Fig. 7). Going from **2** to **2b** and **2c**, just slight changes to the geometrical parameters are observed. For instance, the Ru–NO bond distance changes from 1.762 to 1.782 and 1.772 Å, respectively. On the other hand, the energy decomposition analysis provide more significant results (Fig. 8), indicating that the

NO^+ group binds more strongly in **2** than in **2b** and **2c**. The relative $\Delta\Delta E_{int}$ values are approximately 13.0 and 14.0 kcal mol^{-1} for **2b** and **2c**, respectively. The less stable bonding situation can be attributed, in particular, not only to the increase of the relative electrostatic component (in both **2b** and **2c**), but also to the Pauli repulsion term, $\Delta\Delta E_{Pauli}$, which increases when going directly from **2** to **2c**. Therefore, as expected, the Ru–NO bonding situation prior to and after the $\{RuNO\}^6$ to $\{RuNO\}^7$ core reduction will be affected by the nature of the heteroatoms in macrocyclic tetracoordinated ligands.

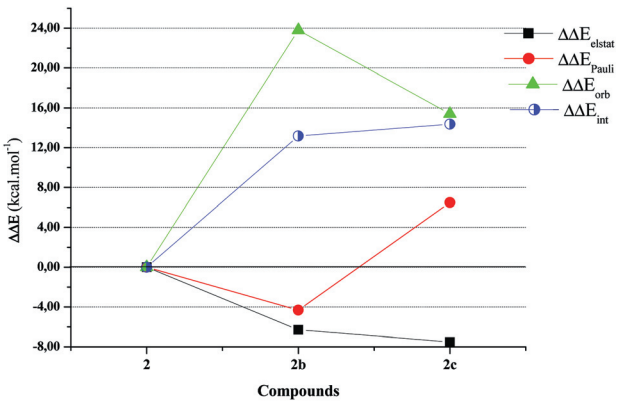

Fig. 8 Relative energy decomposition analysis (kcal mol^{-1}) for compounds **2**, **2b**, and **2c**.

EDA of *trans*-$[Ru^{II}Cl(NO)(NH_3)_4]^+$ and *trans*-$[Ru^{II}Cl(NO)(mac)]^+$. Experimental results[37] indicate that *trans*-$[Ru(NO)(NH_3)_4(L)]^{q+}$ nitrosyl complexes can undergo a one-electron reduction in solution and, according to MO calculations (DFT),[54,100] the additional electron is localized at the π*NO ligand. For this reason, we performed the EDA for the reduced species, *trans*-$[Ru^{II}Cl(NO)(NH_3)_4]^+$, and extended the procedure to *trans*-$[Ru^{II}Cl(NO)(mac)]^+$, considering as fragments NO^0 and the remaining metal fragments *trans*-$[Ru^{II}Cl(NH_3)_4]^+$ and *trans*-$[Ru^{II}Cl(mac)]^+$ (Table 4).

The EDA results in Table 4 show that the Ru–NO bonds in $\{RuNO\}^7$ species exhibit a considerable decrease in the ΔE_{orb} value, in comparison with the values of the $\{RuNO\}^6$ (Table 3). This decrease in ΔE_{orb} is attributed to a reduction not only in the $\Delta E_{(A')}$ but also (and mainly) in the $\Delta E_{(A'')}$ component. Despite the fact that it is not possible to split the orbital components into σ and π interactions, the reduction in the $\Delta E_{(A')}$ and $\Delta E_{(A'')}$ values can be attributed to the bending of the NO group. As a consequence, a weakening of the Ru–NO bond in $\{RuNO\}^7$ is expected, making the NO^0 ligand more susceptible to dissociation. Indeed, these bonds are weaker after reduction by one electron, as confirmed by the geometrical parameters (Tables 1 and 2), which indicate an increase in the Ru–NO bond lengths. The largest and the smallest values of ΔE_{orb} are observed for the GS and MS1 states, respectively, while MS2 presents an intermediate value. However, not only is the orbital term responsible for weakening of the Ru–NO bond in $\{RuNO\}^7$, but also the ΔE_{Pauli} value, which increases in comparison with these bonds in

Table 4 EDA of axial NO^0 of *trans*-$[Ru^{II}(Cl)NO(NH_3)_4]^+$(**1a**), and *trans*-$[Ru^{II}(Cl)NO(mac)]^+$ complexes (**2a–9a**) at BP86/TZ2P[a]

	1a			2a			3a			4a			5a		
	GS	MS1	MS2	GS	MS1	MS2	GS	MS1	MS2	GS	MS1	MS2	GS	MS1	MS2
	C_s	C_s	C_s	C_s	C_s	C_s	C_s	C_s	C_s	C_s	C_s	C_s	C_s	C_s	C_s
ΔE_{int}	−66.3	−31.1	−54.4	−70.3	−35.0	−55.2	−71.4	−35.7	−58.3	−63.8	−27.7	−42.3	−66.5	−28.6	−45.3
ΔE_{pauli}	163.7	79.9	137.4	172.4	90.6	144.1	173.0	88.6	142.1	178.6	95.1	153.7	174.8	91.3	150.2
ΔE_{elstat}	−98.0	−42.7	−63.7	−101.7	−47.4	−67.1	−103.3	−47.2	−66.9	−101.2	−46.9	−68.3	−100.5	−45.8	−66.2
	43%	38%	33%	44%	38%	34%	41%	38%	33%	42%	38%	35%	42%	38%	33.9%
ΔE_{orb}[b]	−132.0	−68.4	−128.1	−141.0	−78.2	−132.2	−141.2	−77.2	−133.6	−141.2	−75.9	−127.6	−140.8	−74.1	−129.2
	57%	62%	67%	58%	62%	66%	59%	62%	66%	58%	62%	65%	58%	62%	66.1%
$\Delta E_{(A')}$	−75.2	−37.2	−118.4	−78.8	−39.1	−121.5	−79.0	−38.8	−124.2	−79.4	−39.4	−117.0	−80.4	−39.3	−119.2
$\Delta E_{(A'')}$	−56.8	−31.2	−9.7	−62.1	−39.0	−10.8	−62.1	−38.4	−9.4	−61.8	−36.6	−10.7	−60.4	−34.8	−10.0
$-D_e$	−50.9	−17.2	−30.3	−53.5	−20.2	−31.5	−55.0	−21.0	−35.1	−44.1	−10.7	−12.7	−46.7	−12.6	−17.9
ΔE_{prep}	15.4	13.9	24.1	16.8	14.8	23.7	16.4	14.7	23.2	19.7	17.0	29.6	19.8	16.0	27.4
q(f1)[c]	1.30	1.22	1.36	1.35	1.28	1.37	1.35	1.28	1.38	1.34	1.26	1.35	1.32	1.25	1.35
q(f2)	−0.30	−0.22	−0.36	−0.35	−1.28	−0.37	−0.35	−0.28	−0.38	−0.34	−0.26	−0.35	−0.32	−0.25	−0.35

	6a			7a			8a			9a		
	GS	MS1	MS2	GS	MS1	MS2	GS	MS1	MS2	GS	MS1	MS2
	C_s	C_s	C_s	C_s	C_s	C_s	C_s	C_s	C_s	C_s	C_s	C_s
ΔE_{int}	−69.7	−34.5	−51.2	−73.3	−35.4	−57.2	−62.4	−26.9	−38.3	−71.8	−31.0	−47.1
ΔE_{pauli}	172.0	92.7	137.9	168.2	83.7	136.5	176.1	92.9	143.1	172.0	87.4	144.7
ΔE_{elstat}	−102.6	−49.1	−64.0	−101.4	−45.2	−63.7	−101.2	−46.3	−64.0	−100.3	−44.6	−64.0
	43%	39%	34%	42%	38%	33%	42%	39%	35%	41%	38%	33%
ΔE_{orb}[b]	−139.1	−78.0	−125.1	−140.1	−73.9	−130.1	−137.3	−73.5	−117.4	−143.5	−73.7	−127.8
	57%	61%	66%	58%	62%	67%	58%	61%	65%	59%	62%	67%
$\Delta E_{(A')}$	−77.8	−38.9	−115.4	−78.6	−37.7	−121.4	−77.2	−38.1	−108.0	−82.0	−39.0	−118.2
$\Delta E_{(A'')}$	−61.3	−39.2	−9.7	−61.5	−36.3	−8.7	−60.1	−35.5	−9.4	−61.5	−34.7	−9.6
$-D_e$	−51.3	−19.0	−25.5	−55.8	−20.9	−34.1	−42.0	−9.9	−8.1	−50.1	−16.1	−20.6
ΔE_{prep}	18.4	15.5	25.7	17.5	14.5	23.1	20.4	17.0	30.2	21.7	15.6	26.5
q(f1)[c]	1.35	1.28	1.36	1.33	1.25	1.37	1.33	1.26	1.34	1.31	1.24	1.34
q(f2)	−0.35	−1.28	−0.36	−0.33	−0.25	−0.37	−0.33	−0.26	−0.34	−0.31	−0.24	−0.34

[a] Energy contributions in kcal mol^{-1}. [b] Percentage contribution to the total orbital interactions, ΔE_{orb}. [c] Hirshfeld charges for fragments.

{RuNO}^{6}. It is interesting to note that while both non reduced *trans*-[Ru^{II}Cl(NO)(mac)]$^{2+}$ and *trans*-[Ru^{II}(L)(NO)(NH$_3$)$_4$]$^{2+}$ species are very stable with regards to NO release, the rate of release of NO from *trans*-[Ru^{II}Cl(NO)(mac)]$^+$ is smaller than for *trans*-[Ru^{II}(L)(NO)(NH$_3$)$_4$]$^+$.[37]

Even after the reduction, macrocyclic complexes in the GS, **2a–9a**, exhibit more negative values of ΔE_{int} than **1a**, indicating that even NO^0 bonds more strongly with complexes containing tetraazamacrocycle ligands than with those containing tetraamines. However, some exceptions are observed. For example, *N*-substituted tetraazamacrocycles such as **4a**, **5a**, and **8a**, depending on the state under consideration, can exhibit ΔE_{int} values smaller than those observed for **1a**. This difference occurs mainly due to an increase in the Pauli repulsion term, ΔE_{Pauli} and a small decrease in the orbital term, ΔE_{orb}. The bond energy dissociation values, $-D_e$, also confirm this trend. Therefore, the EDA results suggest that not only the size of the tetraazamacrocycle employed but also the nature of the substituents of *N*-substituted tetraazamacrocycles can affect the nature of the Ru–NO bonds in {RuNO}^{6} and {RuNO}^{7} species. This study not only demonstrates the importance of exploring new substituents in equatorial macrocyclic ligands, but also indicates that the ring size can be significant in terms of the release of the NO^0 group.

Summary and conclusions

The structures of the ground state GS and light-induced metastable states MS1 and MS2, obtained for *trans*-[Ru^{II}Cl(NO)(NH$_3$)$_4$]$^{2+}$, *trans*-[Ru^{II}Cl(NO)(mac)]$^{2+}$, *trans*-[Ru^{II}Cl(NO)(NH$_3$)$_4$]$^+$, and *trans*-[Ru^{II}Cl(NO)(mac)]$^+$ complexes, characterize the nitrosonium and nitrosyl character of the NO group, before and after one-electron reduction, respectively. The calculated vibrational frequencies reproduce very well the chemical characteristics of the NO$^+$ and NO^0 groups. The geometrical parameters also indicate that complexes with tetraazamacrocycles as equatorial ligands exhibit an increase in the Ru–Cl bond length and contraction of the Ru–NO, Ru–ON, and Ru–N(*i*) bonds. This behavior is observed not only prior to but also after the reduction by one electron of the NO group. In the presence of tetraazamacrocycles as equatorial ligands, the Ru–Cl bonds become weak while the Ru–NO, Ru–ON, and Ru–N(*i*) bonds become stronger.

In general, the EDA results indicate that in the presence of tetraazamacrocyclic ligands, the NO$^+$ and NO^0 groups bind more strongly with the metal centre than in the presence of common tetraamines, which is in agreement with the lower NO release rate constants expected for such ligands and experimentally observed for **2**. Also, the degree of Ru$_{d\pi-\pi^*}$NO back-donation of the tetraazamacrocycle complexes is higher than that of *trans*-[Ru^{II}Cl(NO)(NH$_3$)$_4$]$^{2+}$, which should reflect in the NO electrophilicity. In addition, the results also indicate that not only the size of the tetraazamacrocycle employed but also the nature of the substituents of *N*-substituted tetraazamacrocycles can affect the nature of the Ru–NO bond in {RuNO}^{6} and {RuNO}^{7} complexes, thus affecting its chemical properties. This study not only highlights the importance of exploring new *N*-substituted tetraazamacrocycles as equatorial ligands, but also indicates that the ring size can be significant in terms of the release of the NO^0 group. EDA have also revealed that Ru–NO bonding situation prior to and after the {RuNO}^{6} to {RuNO}^{7} core reduction will be affected by the nature of the heteroatoms in macrocyclic tetracoordinated ligands.

By further exploring such approaches, new ruthenium nitrosyl complexes could be synthesized as NO–prodrugs with potential biological applications.

Acknowledgements

G. F. Caramori thanks FAPESC and CNPq for the financial support (Processo n°. 17.413/2009-0). A. G. Kunitz and K. F. Andriani thank CNPq and CAPES, F. G. Doro thanks FAPESB (Processo PPP039/2010). E. Tfouni thanks CAPES, CNPq and FAPESP (Processo 2006/53266-4). The authors thank the computer center at HRZ Marburg for the excellent service and computational time provided.

References

1 C. Nathan, *FASEB J.*, 1992, **6**, 3051.
2 E. Culotta and D. E. Koshland, *Science*, 1992, **258**, 1861.
3 Y. Noda, A. Mori, R. Liburdy and L. J. Packer, *J. Pineal Res.*, 1999, **27**, 159.
4 V. Retttori, N. Belova, W. L. Dees, C. L. Nyberg, M. Gimeno and S. M. McCann, *Proc. Natl. Acad. Sci. U. S. A.*, 1993, **90**, 10130.
5 B. J. R. Whittle, *Histochem. J.*, 1995, **27**, 727.
6 S. Moncada, R. M. J. Palmer and A. Higgs, *Pharmacol. Rev.*, 1991, **43**, 109.
7 L. J. Ignarro, *Nitric Oxide: Biology and Pathobiology*, Academic Press, San Diego, CA, 2000.
8 V. Bauer and R. Sotníkova, *Gen. Physiol. Biophys.*, 2010, **29**, 319.
9 L. J. Ignarro, G. M. Buga, K. S. Wood, R. E. Byrns and G. Chaudhuri, *Proc. Natl. Acad. Sci. U. S. A.*, 1987, **84**, 9265.
10 R. F. Furchgott, *Angew. Chem., Int. Ed.*, 1999, **38**, 1870.
11 S. A. Waldman and F. Murad, *Pharmacol. Rev.*, 1987, **39**, 163.
12 D. A. Wink, H. B. Hines, R. Y. S. Cheng, C. H. Switzer, W. Flores-Santana, M. P. Vitek and L. A. Ridnour, *J. Leukocyte Biol.*, 2011, **89**, 873.
13 Literature search using the keyword "nitric oxide" results today in over 10 000 publications, a large number compared with the hundreds in the 80s.
14 D. A. Wink and J. B. Mitchell, *Free Radical Biol. Med.*, 1998, **25**, 434.
15 Y. X. Wang, P. Legzdins, J. S. Poon and C. Y. J. Pang, *J. Cardiovasc. Pharmacol.*, 2000, **35**, 73.
16 S. P. Fricker, *Platinum Metals Rev.*, 1995, **39**, 150.
17 S. P. Fricker, E. Slade, N. A. Powell, O. J. Vaughan, G. R. Henderson, B. A. Murrer, I. L. Megson, S. K. Bisland and F. W. Flitney, *Br. J. Pharmacol.*, 1997, **122**, 1441.
18 N. A. Davies, M. T. Wilson, E. Slade, S. P. Fricker, B. A. Murrer, N. A. Powell and G. R. Henderson, *Chem. Commun.*, 1997, 47.
19 F. G. Marcondes, A. A. Ferro, A. S. Torsoni, M. Sumitani, M. J. Clarke, D. W. Franco, E. Tfouni and M. H. Krieger, *Life Sci.*, 2002, **70**, 2735.
20 D. Bonaventura, R. L. Galvão, J. A. Vercesi, R. S. Silva and L. M. Bendhack, *Vasc. Pharmacol.*, 2007, **46**, 215.
21 I. Szundi, M. J. Rose, I. Sen, A. A. Eroy-Reveles, P. K. Mascharak and O. Einarsdottir, *Photochem. Photobiol.*, 2006, **82**, 1377.
22 E. Tfouni, F. G. Doro, L. E. Figueiredo, J. M. C. Pereira, G. Metzker and D. W. Franco, *Curr. Med. Chem.*, 2010, **17**, 3643.
23 A. D. Ostrowski, S. J. Deakin, B. Azhar, T. W. Miller, N. Franco, M. M. Cherney, A. J. Lee, J. N. Burstyn, J. M. Fukuto, I. L. Megson and P. C. Ford, *J. Med. Chem.*, 2010, **53**, 715.
24 A. D. Ostrowski and P. C. Ford, *Dalton Trans.*, 2009, 10660.
25 A. D. Pereira, P. C. Ford, R. S. da Silva and L. M. Bendhack, *Nitric Oxide*, 2011, **24**, 192.
26 G. M. Halpenny, K. R. Gandhi and P. K. Mascharak, *ACS Med. Chem. Lett.*, 2010, **1**, 180.

27 G. Von Poelhsitz, A. L. Bogado, M. P. de Araujo, H. S. Selistre-De-Araujo, J. Ellena, E. E. Castellano and A. A. Batista, *Polyhedron*, 2007, **26**, 4707.
28 P. C. Ford, J. Bourassa, K. Miranda, B. Lee, I. Lorkovic, S. Boggs, S. Kudo and L. Laverman, *Coord. Chem. Rev.*, 1998, **171**, 185.
29 J. A. Olabe, *Dalton Trans.*, 2008, 3633.
30 S. Y. Shaban and R. van Eldik, *Eur. J. Inorg. Chem.*, 2010, **4**, 554.
31 P. G. Wang, M. Xian, X. P. Tang, X. J. Wu, Z. Wen, T. W. Cai and A. J. Janczuk, *Chem. Rev.*, 2002, **102**, 1091.
32 J. A. McCleverty, *Chem. Rev.*, 2004, **104**, 403.
33 M. J. Rose and P. K. Mascharak, *Coord. Chem. Rev.*, 2008, **252**, 2093.
34 J. J. N. Silva, W. R. Pavanelli, J. C. M. Pereira, J. S. Silva and D. W. Franco, *Antimicrob. Agents Chemother.*, 2009, **53**, 4414.
35 P. M. M. Guedes, F. S. Oliveira, F. R. S. Gutierrez, G. K. da Silva, G. J. Rodrigues, L. M. Bendhack, D. W. Franco, M. A. D. Matta, D. S. Zamboni, R. S. da Silva and J. S. Silva, *Br. J. Pharmacol.*, 2010, **160**, 270.
36 E. Tfouni, F. G. Doro, A. S. Gomes, R. S. da Silva, G. Metzker, P. G. Z. Benini and D. W. Franco, *Coord. Chem. Rev.*, 2010, **254**, 355.
37 E. Tfouni, M. Krieger, B. R. McGarvey and D. W. Franco, *Coord. Chem. Rev.*, 2003, **236**, 57.
38 E. Tfouni, K. Q. Ferreira, F. G. Doro, R. S. Silva and Z. N. da Rocha, *Coord. Chem. Rev.*, 2005, **249**, 405.
39 D. R. Lang, J. A. Davis, L. G. F. Lopes, A. A. Ferro, L. C. G. Vasconcellos, D. W. Franco, E. Tfouni, A. Wieraszko and M. J. Clarke, *Inorg. Chem.*, 2000, **39**, 2294.
40 F. D. Oliveira, K. Q. Ferreira, D. Bonaventura, L. M. Bendhack, A. C. Tedesco, S. D. Machado, E. Tfouni and R. S. da Silva, *J. Inorg. Biochem.*, 2007, **101**, 313.
41 R. M. Carlos, A. A. Ferro, H. A. S. Silva, M. G. Gomes, S. S. S. Borges, P. C. Ford, E. Tfouni and D. W. Franco, *Inorg. Chim. Acta*, 2004, **357**, 1381.
42 F. Bottomley, *Acc. Chem. Res.*, 1978, **11**, 158.
43 F. Paulat, T. Kuschel, C. Nather, V. K. K. Praneeth, O. Sander and N. Lehnert, *Inorg. Chem.*, 2004, **43**, 6979.
44 D. K. Cabbiness and D. W. Margerum, *J. Am. Chem. Soc.*, 1969, **91**, 6540.
45 X. Liang and P. J. Sadler, *Chem. Soc. Rev.*, 2004, **33**, 246.
46 E. K. Barefield, G. M. Freeman and D. G. Van Derveer, *Inorg. Chem.*, 1986, **25**, 552.
47 D. J. Szalda, E. Fujita, R. Sanzenbacher, H. Paulus and H. Elias, *Inorg. Chem.*, 1994, **33**, 5857.
48 G. E. Collins, L. S. Choi and J. H. Callhan, *J. Am. Chem. Soc.*, 1998, **120**, 1474.
49 G. J. Bridger, R. T. Skerlj, D. Thornton, S. Padmanabhan, S. A. Martellluccci, G. W. Henson, M. J. Abrams, N. Yamamoto, K. De Vreese, R. Auwels and E. J. De Clercq, *J. Med. Chem.*, 1995, **38**, 366.
50 J. A. Esté, *Acta Biomed. Lovaniensia*, 1999, **190**, 1.
51 D. Schols, J. A. Esté, G. Henson and E. J. De Clercq, *Antiviral Res.*, 1997, **35**, 1147.
52 D. Schols, S. Struyf, J. Van Damme, J. A. Esté, G. Henson and E. J. De Clercq, *J. Exp. Med.*, 1997, **186**, 1383.
53 J. C. Toledo Jr., L. G. F. Lopes, A. A. Alves, L. P. Silva and D. W. Franco, *J. Inorg. Biochem.*, 2002, **89**, 267.
54 G. F. Caramori and G. Frenking, *Organometallics*, 2007, **26**, 5815.
55 G. F. Caramori and G. Frenking, *Croat. Chim. Acta*, 2009, **82**, 219.
56 F. G. Doro, E. E. Castellano, L. A. B. Moraes, M. N. Eberlin and E. Tfouni, *Inorg. Chem.*, 2008, **47**, 4118.
57 F. G. Doro, I. M. Pepe, S. E. Galembeck, R. M. Carlos, Z. N. da Rocha, M. Bertotti and E. Tfouni, *Dalton Trans.*, 2011, **40**, 6420.
58 K. Q. Ferreira and E. Tfouni, *J. Braz. Chem. Soc.*, 2010, **21**, 1349.
59 P. C. Ford, *Acc. Chem. Res.*, 2008, **41**, 190.
60 F. Roncaroli, M. E. Ruggiero, D. W. Franco, G. L. Estiu and J. A. Olabe, *Inorg. Chem.*, 2002, **41**, 5760.
61 F. Roncaroli, M. Videla, L. D. Slep and J. A. Olabe, *Coord. Chem. Rev.*, 2007, **1251**, 903.
62 N. L. Fry and P. K. Mascharak, *Acc. Chem. Res.*, 2011, **44**, 289.
63 M. A. Marti, D. A. Scherlis, F. A. Doctorovich, P. Ordejon and D. A. Estrin, *JBIC, J. Biol. Inorg. Chem.*, 2003, **8**, 595.
64 P. O. Whimp, M. F. Bailey and N. F. J. Curtis, *J. Chem. Soc. A*, 1970, 1956.
65 P. J. Connolly and E. J. Billo, *Inorg. Chem.*, 1987, **26**, 3224.
66 M. A. Donnelly and M. Zimmer, *Inorg. Chem.*, 1999, **38**, 1650.
67 K. Q. Ferreira, F. G. Santos, Z. N. da Rocha, T. Guaratini, R. S. da Silva and E. Tfouni, *Inorg. Chem. Commun.*, 2004, **7**, 204.
68 K. Q. Ferreira, L. N. Cardoso, S. Nikolaou, Z. N. da Rocha, R. S. da Silva and E. Tfouni, *Inorg. Chem.*, 2005, **44**, 5544.
69 D. V. Fomitchev, I. Novozhilova and P. Coppens, *Tetrahedron*, 2000, **56**, 6813.
70 C. Kim, I. Novozhilova, M. S. Goodman, K. A. Bagley and P. Coppens, *Inorg. Chem.*, 2000, **39**, 5791.
71 U. Hauser, V. Oestreich and H. D. Z. Rohrweck, *Phys. A*, 1977, **280**, 17.
72 U. Hauser, V. Oestreich and H. D. Z. Rohrweck, *Phys. A*, 1977, **280**, 125.
73 H. Zöllner, Th. Woike, W. Krasser and S. Z. Haussühl, *Z. Kristallogr.*, 1989, **188**, 139.
74 P. Coppens, I. Novozhilova and A. Kovalevsky, *Chem. Rev.*, 2002, **102**, 861.
75 T. E. Bitterwolf, *Coord. Chem. Rev.*, 2006, **250**, 1196.
76 P. Coppens, *Synchrotron Radiat. News*, 1997, **10**, 26.
77 Th. Woike, H. Zöllner, W. Krasser and S. Haussühl, *Solid State Commun.*, 1990, **73**, 149.
78 Th. Woike and S. Haussühl, *Solid State Commun.*, 1993, **86**, 333.
79 S. C. da Silva and D. W. Franco, *Spectrochim. Acta, Part A*, 1999, **55**, 1515.
80 B. Cormary, I. Malfant, M. B. L. Cointe, L. Toupet, B. Delley, D. Schaniel, N. Mockus, Th. Woike, K. Fejfarova, V. Petricek and M. Dusek, *Acta Crystallogr., Sect. B: Struct. Sci.*, 2009, **65**, 612.
81 A. D. Becke, *Phys. Rev. A: At., Mol., Opt. Phys.*, 1989, **38**, 3098.
82 J. P. Perdew, *Phys. Rev. B*, 1986, **33**, 8822.
83 J. G. Snijders, E. J. Baerends and P. Vernooijs, *At. Data Nucl. Data Tables*, 1982, **26**, 483.
84 J. Krijn and E. J. Baerends, Fit Functions in the HFS Method, Internal Report (in Dutch), Vrije Universiteit, Amsterdam, 1984.
85 E. van Lenthe, E. J. Baerends and J. G. Snijders, *J. Chem. Phys.*, 1993, **99**, 4597.
86 E. van Lenthe, E. J. Baerends and J. G. Snijders, *J. Chem. Phys.*, 1996, **105**, 6505.
87 E. van Lenthe, R. van Leeuwen, E. J. Baerends and J. G. Snijders, *Int. J. Quantum Chem.*, 1996, **57**, 281.
88 F. M. Bickelhaupt and E. J. Baerends, *Rev. Comput. Chem.*, 2000, **15**, 1.
89 G. te Velde, F. M. Bickelhaupt, E. J. Baerends, S. J. A. van Gisbergen, C. F. Guerra, J. G. Snijders and T. Ziegler, *J. Comput. Chem.*, 2001, **22**, 931.
90 M. Lein and G. Frenking, *Theory and Applications of Computational Chemistry: The First 40 Years*, ed. C. E. Dykstra, G. Frenking, K. S. Kim and G. E. Scuseria, Elsevier, Amsterdam, 2005, p. 291.
91 K. Morokuma, *J. Chem. Phys.*, 1971, **55**, 1236.
92 K. Morokuma, *Acc. Chem. Res.*, 1977, **10**, 294.
93 T. Ziegler and A. Rauk, *Theor. Chim. Acta*, 1977, **46**, 1.
94 C. Esterhuysen and G. Frenking, *Theor. Chem. Acc.*, 2004, **111**, 381.
95 A. Kovács, C. Esterhuysen and G. Frenking, *Chem.–Eur. J.*, 2005, **11**, 1813.
96 G. Frenking, K. Wichmann, N. Fröhlich, C. Loschen, M. Lein, J. Frunzke and V. M. Rayón, *Coord. Chem. Rev.*, 2003, **55**, 238.
97 G. Frenking and N. Fröhlich, *Chem. Rev.*, 2000, **55**, 717.
98 W. Heitler and F. London, *Z. Phys.*, 1979, **44**, 455.
99 I. B. Bersuker, *Electronic Structure and Properties of Transition Metal Compounds*, 1st edn, John Wiley & Sons, 1995.
100 S. I. Gorelsky, S. C. da Silva, A. B. P. Lever and D. W. Franco, *Inorg. Chim. Acta*, 2000, **300**, 698.
101 J. H. Enemark and R. D. Feltham, *Coord. Chem. Rev.*, 1974, **13**, 339.
102 G. B. Richter-Addo and P. Legzdins, *Metal Nitrosyls*, Oxford University Press, New York, 1st edn, 1992.
103 J. Bordini, D. O. Novaes, I. E. Borissevitch, B. T. Owens, P. C. Ford and E. Tfouni, *Inorg. Chim. Acta*, 2008, **361**, 2252.
104 L. E. Goodrich, F. Paulat, V. K. K. Praneeth and N. Lehnert, *Inorg. Chem.*, 2010, **49**, 6293.
105 A. F. Schreiner, S. W. Lin, P. J. Hauser, E. A. Hocpus, D. J. Hamm and J. D. Gukter, *Inorg. Chem.*, 1972, **11**, 880.
106 The open-shell fragments for the EDA can only be calculated with the ADF program by using the restricted formalism while for the optimization of the fragments the unrestricted formalism is used. The energy differences between the restricted and unrestricted calculations are below 1 kcal mol^{-1} and are incorporated into the ΔE_{prep} values.
107 D. W. Pipes and T. J. Meyer, *Inorg. Chem.*, 1984, **23**, 2466.
108 J. C. Toledo, H. A. S. Silva, M. Scarpellini, V. Miori, A. J. Camargo, M. Bertotti and D. W. Franco, *Eur. J. Inorg. Chem.*, 2004, 1879.
109 B. R. McGravey, A. A. Ferro, E. Tfouni, C. W. Bezerra, I. Bagatin and D. W. Franco, *Inorg. Chem.*, 2000, **39**, 3577.

110 R. G. Serres, C. A. Grapperhaus, E. Bothe, E. Bill, T. Weyhermuller, F. Neese and K. Wieghardt, *J. Am. Chem. Soc.*, 2004, **126**, 5138.
111 J. C. Patterson, I. M. Lorkovic and P. C. Ford, *Inorg. Chem.*, 2003, **42**, 4902.
112 F. Roncaroli, L. M. Baraldo, L. D. Slep and J. A. Olabe, *Inorg. Chem.*, 2002, **41**, 1930.
113 H. A. Jahn and E. Teller, *Proc. R. Soc. London, Ser. A*, 1937, **161**, 220.
114 H. A. Jahn, *Proc. R. Soc. London, Ser. A*, 1938, **164**, 117.
115 N. Lehnert, J. T. Sage, N. Silvernail, W. R. Scheidt, E. E. Alp, W. Sturhahn and J. Zhao, *Inorg. Chem.*, 2010, **49**, 7197.
116 F. L. Hirshfeld and S. Rzotkiewicz, *Mol. Phys.*, 1974, **27**, 1319.